Peer reviewed version

Modular simulation framework for Electro-ribbon Actuators

Bruno Castro, Richard Suphapol Diteesawat, Majid Taghavi, and Jonathan Rossiter

Abstract— The Electro-ribbon Actuator (ERA) is a new class of soft robotic actuator that is light weight, low cost and has high contraction strain. The combination of compliance and dielectrophoretic liquid zipping introduces significant nonlinearity to the ERA and makes modelling challenging. This article introduces a lumped-parameter model (LPM) to simulate the actuation behavior and performance of ERAs. The ERA is made of two flexible opposite insulated electrodes attached together at both ends. The application of a bead of liquid dielectric to the attaching points of the electrodes provides a large force amplification and enables high contraction over 99% and high force-to-weight ratio. The proposed method can simulate a flexible and deformable beam, the main structure of the ERA, predicting the ERA's deformation under external loads with $< 5\%$ errors. It computes the electrostatic force generated between two electrodes and simulates the zipping behaviour. A multiphysics finite element analysis has been performed to validate the model and, a comparison is show with the experimental data in a series of stationary and time-dependent tests. This work provides a rapid route to design and modelling of future soft robots and soft machines.

I. INTRODUCTION

Recent years have seen a prominent development in soft robotics [1], [2], with promising applications emerging in various fields ranging from health technologies to human-machine interaction and agriculture [3], [4]. One of the open challenges in soft robotics remains the gap between simulation and reality [5]. Efforts have been put into developing accurate models to simulate the behavior of soft components and accurate numerical models and simulation libraries and databases for soft mechanisms and materials [6], [7]. However, design and control of soft robots are still dominated by labour-intensive trial-and-error processes, and needs a computational framework capable of aiding in the formal design, control and experimental analysis of soft robotics [8].

Early efforts to simulate soft systems relied on the application of Finite Elements (FE) methods whilst recent advances in the adaptation of simulation techniques from the computer graphics community into robotics has enabled the dynamic simulation of soft materials. Examples include voxel-based simulations [9], and more recently mass-spring models based on discrete differential geometry, which have led to faster than real-time performance on single thread desktop processors [8].

Moreover the simulation of soft stimuli-responsive components becomes more challenging when external nonlinear forces (e.g. magnetic or electrostatic forces) are present [10]. FE methods are commonly used to solve this kind of problems through commercially available programs such as COMSOL and ANSYS [11], [12]. Such solutions involve meshing the geometry and solving a set of partial differential equations that govern the dynamics of the system defined by fundamental theories. Recent alternatives to FE to solve the efficiency problem include deep learning driven simulations [12], and the discretization of well-established models of continuous elastic Kirchhoff rods in the realm of computer graphics [8], [13], [14]. However, none of these faster methods include actuation force (e.g. electrostatic force) and are insufficient to model soft actuators..

Faster simulations, achieved through lumped-parameter models (LPM), have been commonly found in circuit or fluid modelling, in applications as varied as ion-battery modelling [15] and cardiovascular blood flow [16], [17]. When applied to mechanical systems LPMs typically break down the mechanical system into a set of rigid bodies connected by springs and dampers, known as kinematic pairs, that control the relative motion between the rigid bodies [18]. LPMs or mass-spring-type systems, have also been used to model flexible robotic arms [19], animal skin [20], the mechanics and deformations in a car crash collision [21], and in some cases with faster than real-time simulation [8].

The Electro-ribbon Actuators (ERA), shown in Figure 1, is a flexural actuator that operates on the Dielectrophoretic Liquid Zipping (DLZ) concept [22]. The actuator consists of two flexible insulated electrodes, clipped together at both ends, and displaced by the application of an external load. A small droplet of dielectric liquid is added to the zipping points of the ERA to amplify the attractive electrostatic force between the electrodes, theoretically up to 120-folds. When a high voltage is applied between the electrodes, the electrostatic force concentrates at the zipping points,

B. Castro, R. S. Diteesawat, M. Taghavi, and J. Rossiter are with the Department of Engineering Mathematics, University of Bristol, Bristol, BS8 1BU and Bristol Robotics Laboratory, Bristol, BS16 1QY, UK (email: ul18363@bristol.ac.uk, richard.diteesawat@bristol.ac.uk, majid.taghavi@bristol.ac.uk, jonathan.rossiter@bristol.ac.uk). Corresponding author: Majid Taghavi.
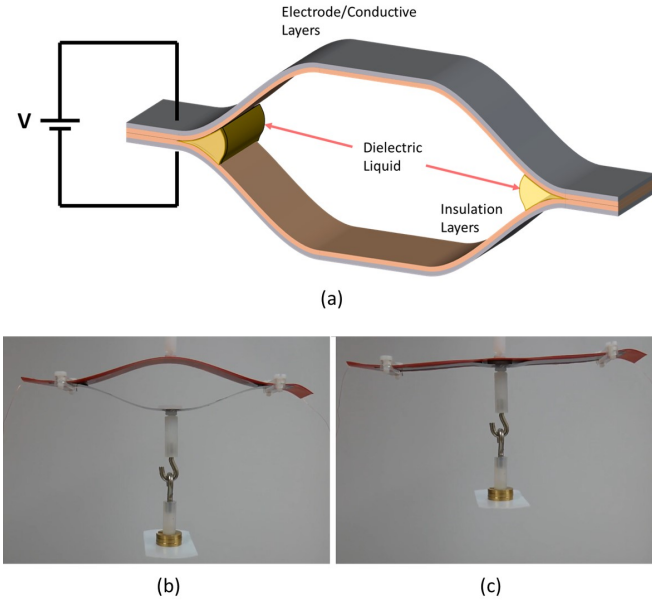
Fig. 1. Top: (a) Diagram of the ERA. Bottom: Physical ERA (b) turned off/relaxed and (c) powered and fully zipped.

resulting in contraction and progressive zipping along the actuator until both electrodes come into contact along their lengths.

This actuator has shown high contraction (up to 99.8% of the fully extended length of the actuator), high force-to-weight ratio (>1000 times its own weight), and high power (equivalent to human muscle) [22]. These capabilities, the flexural body, and the accessibility of the input electric signal make this actuator a potential powerful candidate for soft robotics applications including deployable structures and origami robots for various uses including locomotion, gripper and solar panels. Despite its intrinsic self-sensing properties [23],the complex non-linearity of the actuator, its compliance and inherent pull-in instability make the control of the actuator difficult. Although a modified PID control was implemented to operate the ERA [24], a precise simulation predicting its actuation behaviour under different configurations is required to improve its performance and efficiently design for various applications.

In this paper, a model is proposed to simulate an ERA which is actuated by electrostatic forces based on a mass-spring mechanical simulation model and the estimation of the shape of the continuous beam through cubic Bezier curves which numerically integrate the electrostatic forces along the actuator surface. The proposed model is then compared with FE results computed by the multi-physics simulation software (COMSOL) and experimental data.

The paper is structured as follows: In Section II the proposed model is described, followed by simulation results compared with the experimental data in Section III. Sections IV and V discuss the results and draw conclusions.

II. Proposed Model

In order to study the ERA behavior, the actuator is simulated with two planes: a mechanical plane where the geometry and the dynamics of the actuator are calculated, and an electrostatic plane where the electrostatic forces exerted by the actuator are analyzed.

A. Mechanical modelling

The mechanical model approximates each electrode of the actuator as a set of linked particles, exerting a mechanical force over adjacent particles based on their local geometry, as shown in Figure 2. The simulation starts by defining an initial kinematic configuration of the linked particles, defining the initial positions ($p_{i,o}$), instantaneous velocities ($v_{i,o}$) and accelerations ($a_{i,o}$) of each particle ($i \in \{0, 1, 2, ..., N\}$), expressed in a global reference frame. A recommended starting configuration in modelling the shape of a electrode with length (L), thickness (b), width (w), and N particles is to distribute the particles uniformly along L.

The simulation cycle, represented in Figure 3, consists of (1) calculating the mechanical and electrostatic forces applied on each particle, i, (2) sizing the timestep to avoid instabilities and (3) applying the calculated timestep and forces to compute the acceleration (a_i), velocity (v_i), position (p_i) and relative positions between particle pairs (dp_i) of the next iteration. These parameters can be calculated using equation (1), where F_i, m_i and dt are the total force exerted on particle i, the mass of particle i and the timestep, respectively.

$$\vec{a}_i = \frac{\vec{F}_i}{m_i}$$
$$\vec{v}_i(t) = \vec{v}_i(t - dt) + \vec{a}_i(t) * dt \qquad (1)$$
$$\vec{p}_i(t + dt) = \vec{p}_i(t) + \vec{v}_i(t) * dt$$
$$\vec{dp}_{i \to i+1} = \vec{p}_{i+1} - \vec{p}_i$$

The mechanical forces simulated in the model can be divided into (1) direct forces, (2) shear forces, and (3) external damping and loads, which are implemented as follows.
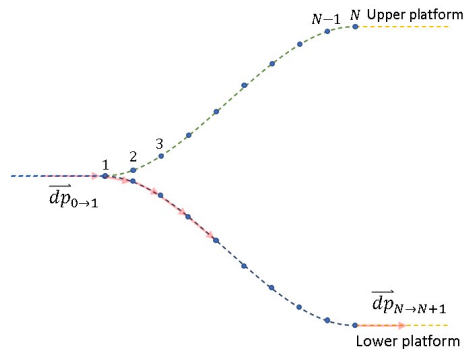

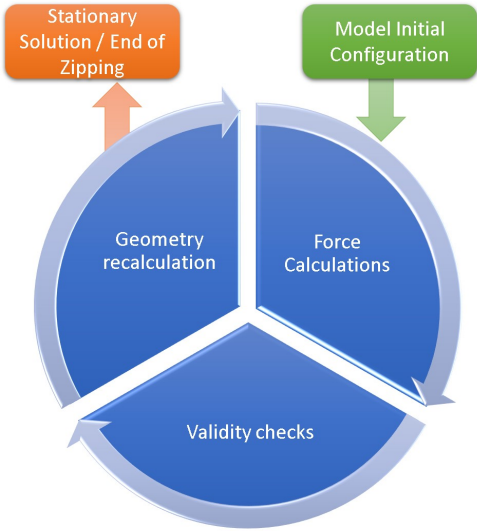Fig. 2. Left half of the actuator approximated by N particles.

Fig. 3. Simulation loop

Fig. 4. Illustration of direct force (F_D) from "i" to "$i+1$", and the shear displacements with respect to the unstressed positions $\Delta\vec{y}_{rel(i+1,i)}$ and $\Delta\vec{y}_{rel(i,i+1)}$.

1) *Direct mechanical forces:* Direct forces act to conserve the relative distance between adjacent particles, dp_i, and are modelled as simple springs with elastic constant, K_D, calculated from the cross sectional area (A), Young Modulus (E), length of the beam (L) and the number of particles in the model (N) in equation (2). Hence, the direct force, F_D, exerted from particle i to $i+1$ is expressed in equation (3).

$$K_D = \frac{A * E * (N-1)}{L} \qquad (2)$$

$$\vec{F}_{D(i\rightarrow i+1)} = -K_D * (|\vec{dp}_i| - \frac{L}{(N-1)})\frac{\vec{dp}_i}{|\vec{dp}_i|} \qquad (3)$$

2) *Shear mechanical forces:* Shear forces act to conserve a local deflection applied perpendicular to the direction of the beam. Shear is directly proportional to the displacement of the particle $i+1$ in its unstressed position with respect to particle i ($\Delta\vec{y}_{rel(i\rightarrow i+1)}$) and of the particle i in its unstressed position with respect to particle $i+1$ ($\Delta\vec{y}_{rel(i+1\rightarrow i)}$), which are derived as as shown in Figure 4.

Shear forces on the particle i due to $\Delta\vec{y}_{rel(i+1\rightarrow i)}$ ($\vec{F}_{S(i+1\rightarrow i)}$) and on the particle $i+1$ from $\Delta\vec{y}_{rel(i\rightarrow i+1)}$ ($\vec{F}_{S(i\rightarrow i+1)}$), are calculated using equation (4), where K_S is the shear elastic coefficient.

$$\begin{aligned}\vec{F}_{S(i\rightarrow i+1)} &= -K_S * \Delta\vec{y}_{rel(i\rightarrow i+1)} \\ \vec{F}_{S(i+1\rightarrow i)} &= -K_S * \Delta\vec{y}_{rel(i+1\rightarrow i)}\end{aligned} \qquad (4)$$

As shown in Figure 4, the local direction of the beam is defined as (i.) the direction immediately before the particles for the shear forces exerted to the right particles, and (ii.) the direction of the beam after the particle pairs for forces applied on the left particles, where ϕ_i is a bending angle of the two adjacent particles.
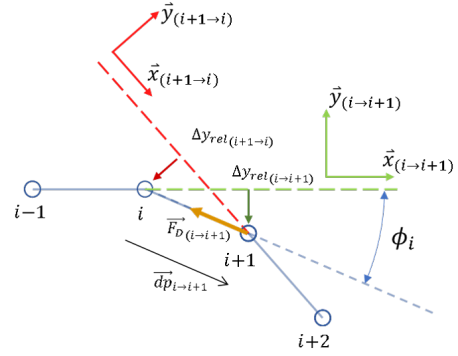
For the edge particles, the beam is set to be in horizontal direction.

It can be deduced that the potential energy of the shear forces converge to the bending energy as reported in the discrete Kirchhoff rod model [13], in the limit of small bending angles ($\phi_i << 1$) and homogeneous spacing between particles ($|\vec{dp}_{i\rightarrow i+1}| \cong |\vec{dp}_{i+1\rightarrow i+2}|, \forall i$), when K_S is set to $\frac{\alpha}{2|\vec{dp}_{i\rightarrow i+1}|^3}$, where α is the bending coefficient.

3) *Damping and Load:* The damping force ($\vec{F}_{Dp_i}$) is calculated with respect to the absolute velocity of each particle, which contrasts to the internal damping considered in other LPM. It can be calculated using equation (5) with an arbitrary damping constant "c".

$$\vec{F}_{Dp_i} = -c|\vec{v}_i|^2\hat{v}_i \qquad (5)$$

To initialize the ERA actuation, an external load is applied at the middle of the ERA to separate the electrodes. The influence of the attached load to the actuator is modelled by increasing the mass of the particles (m_i) where the load ($M_{load,i}$) is attached using equation (6).

$$\vec{m}_i = \frac{M_{electrode}}{2N} + M_{load,i} \qquad (6)$$

B. *Electrical force modelling*

The proposed electrostatic force model simplifies the actuator as a sequence of infinitesimal parallel-plates capacitors [22], with a vertical distance between the plates, $h(x)$ on the horizontal axis, x, at every dx length, as shown in Figure 5. This model is referred in this article as the Parallel-Plates (PP) model.

The continuous shape of the electrode is estimated by fitting a cubic Bezier curve over the position of the particles, since this allow us to generate a differential surface from a set of discrete points and thus calculate a distributed force over the internal surfaces of the actuator. The magnitude of the distributed electrostatic
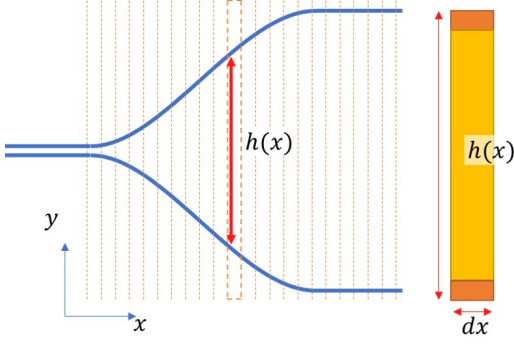
Fig. 5. Electrostatic parallel-plates idealization.

force ($W_{es}(x)$) is calculated through equation (7) and (8) [22].

$$W_{es}(x) = \frac{\varepsilon_{medium}\varepsilon_0 bV^2}{2((\frac{\varepsilon_{medium}}{\varepsilon_{insulator}} - 1)t_{insulator} + h(x))^2} \quad (7)$$

$$W_{es}(x) = \frac{1}{2}\varepsilon_{medium}\varepsilon_0 bE_{breakdown}^2 \quad (8)$$
$$if |E_{breakdown}| < |E_{medium}|$$

Where ε_0 is the electric permittivity of vacuum, ε_{medium} and $\varepsilon_{insulator}$ are the relative electric permittivity of the medium (dielectric liquid) and insulator (PVC tape), and $E_{breakdown}$ is the dielectric breakdown of the medium. E_{medium} is the electric field in the medium, and V is the applied voltage to opposite electrodes. b and $t_{insulator}$ are the electrode's width and the insulator's thickness respectively. The discrete electrostatic force on a particle i is calculated by integrating the distributed force over the continuous shape approximated by the Bezier curve on the interval generated between the position of $i-1$ and i.

C. Time-step size estimation

The last step of the model is estimating the size of the timestep dt, as a validity check to mitigate the risk of divergence in the model. Equation (9) is used to avoid diverging oscillations from numerical errors of damping, direct and shear forces, that may develop into numerical instabilities in the model.

$$dt \leq min(\frac{2m_i}{|\vec{v}_i| * c}, \frac{2|\vec{dp}_i|}{|\vec{v}_i|}, \frac{2|\Delta y_{local,i}|}{|\vec{v}_i|})\forall i \quad (9)$$

III. Simulation Results

Simulations were carried out by modelling an ERA made from two 100 mm long, 12.7 mm wide, 50 μm thick steel electrodes and two layers of 130 μm thick insulators (PVC tape) and with a middle platform of 10 mm long modelled as weightless and perfectly rigid,

using MATLAB as the programming environment and COMSOL to produce and solve FE counterparts.

The simulation is performed by modelling the flexible segments of the left half of the actuator as shown in Fig. 2 with three spatial resolutions of with 21, 61 and 130 particles. The hardware time required by a single thread of an Intel(R) Core(TM)i7-8700 to perform a second of simulation is 6.43 minutes for simulations with 21 particles per sheet with an average timestep of 5.04 μs. This increases to 17.04 minutes and 43.27 minutes for simulations with 61 and 130 particles, respectively, with respective average timesteps of 0.99 μs and 0.49 μs.

K_D is deduced through equation (2) using E as 200GPa, L as 45mm, A as 0.635mm^2, thus computing the values of 56.44, 169.33 and 364.07N/μm for 21, 61 and 130 particles respectively. The damping constant c is chosen experimentally. It affects the simulation timestep size and the drag suffered by the particles in their movement. It was set to 10, 1 and 0.1 for simulations with 21, 61 and 130 particles, respectively, to diminish the overall increase in drag force across the set of particles due to the increased number of particles in the model.

A. Stationary Analysis

The first simulation determines the stationary deformation of the actuator under a range of loads, which will subsequently serve as the initial position before the application of electric field. The procedure of the study is as follows:

1) A model of a flexible beam is built in COMSOL, simulating the conditions of the bottom left quarter of the actuator.
2) A range of loads are applied to the COMSOL model, and the electrode displacement data is recorded.
3) K_S is tuned for the LPM based on one of the configurations to match the displacement of simulation results and experimental data acquired from [22]. See Table I.
4) After calibration of the LPM, a range of loads are applied, and the data of the displacement of the electrode is recorded and then compared with the COMSOL result. See Table II and Figure 6.

B. Contractile Force Validation

The second simulation analysis consists of validating the simulated electrostatic force and its distribution along the surface of the electrodes with empirical data.

Figure 7 shows a typical electrostatic force calculated by the proposed PP model and the corresponding force computed by COMSOL. The PP electrostatic force was significantly lower than the FE results obtained from COMSOL.

A constant scale factor of 6.03 is applied to the PP force result to match the magnitude of the COMSOL result. This scalar has been tested for 27 different simulations with initial displacement of 1, 2, and 4 mm

N	Load [g]	Shear Coefficient	Stroke [mm]	Stroke Error [mm]	Rel. Error	Area Error [mm^2]
21	0	2.4×10^4	0.07	0.0002	0.31%	0.010
61	0	5.8×10^5	0.07	0.0008	1.16%	0.022
130	0	5.6×10^6	0.07	0.0001	0.17%	0.004
21	8	6.4×10^3	2.60	0.0084	0.32%	0.484
61	8	1.5×10^5	2.60	0.0020	0.08%	0.241
130	8	1.5×10^6	2.60	0.0001	0.01%	0.280
21	61	6.0×10^3	17.06	0.0112	0.07%	1.526
61	61	1.4×10^5	17.06	0.0288	0.17%	0.658
130	61	1.4×10^6	17.06	0.0289	0.17%	0.671

TABLE I

Results of calibration of shear coefficient (K_s) for the mechanical LPM model, where stroke represents the distance from the zipping point to the lower platform and stroke error is the comparison between the stroke obtained in COMSOL and the stationary solution obtained from the proposed LPM.

N	Load [g]	Stroke [mm]	Ref. Stroke [mm]	Stroke Error [mm]	Rel. Error	Area Error [mm2]
21	40	12.20	11.94	0.25	2.09%	5.7
61	40	12.26	11.94	0.32	2.58%	7.6
130	40	12.26	11.94	0.31	2.54%	8.0
21	60	16.69	16.84	0.15	0.89%	5.0
61	60	16.83	16.84	0.01	0.06%	0.2
130	60	16.83	16.84	0.01	0.06%	1.1
21	80	20.27	20.87	0.60	2.96%	18.2
61	80	20.46	20.87	0.41	2.02%	10.5
130	80	20.43	20.87	0.45	2.18%	9.0
21	100	23.58	23.84	0.26	1.12%	11.0
61	100	23.34	23.84	0.51	2.17%	13.7
130	100	23.31	23.84	0.53	2.29%	11.1
21	150	28.74	29.53	0.80	2.77%	30.1
61	150	28.21	29.53	1.32	4.68%	38.4
130	150	28.20	29.53	1.34	4.74%	33.6
21	200	31.89	32.80	0.92	2.87%	37.1
61	200	31.19	32.80	1.62	5.18%	49.6
130	200	31.23	32.80	1.57	5.03%	43.0

TABLE II

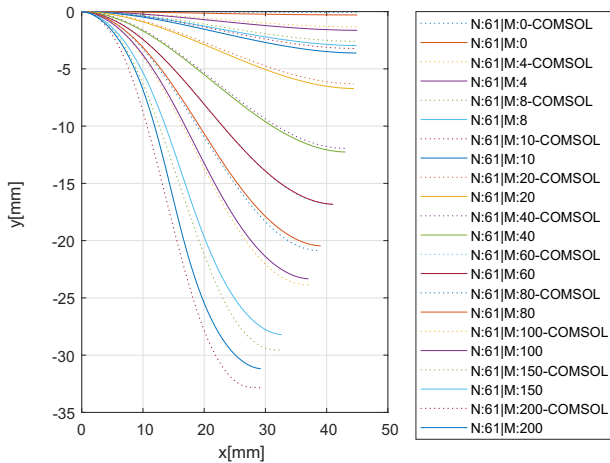Stationary error of mechanical model, where K_s is calibrated at a load of 61 g

Fig. 6. Stationary displacements under different loads after calibration of K_s based on 61 g load, for model with 61 particles.

and a range of voltages between 1 to 12 kV for each displacement. The scale factor of every test was found to be 6.03 with a standard deviation of 0.013. Possible explanations for this scale factor deviation include the calculation of the electrostatic force based on only the opposite differential segment, excluding the effect of adjacent (diagonal) segments.

For this isometric experiment, the electrostatic force is applied to the mechanical model once it reaches equilibrium at an arbitrary separation. The application of the electrostatic force results in progressive zipping and change in mechanical structure until again the system reaches a stationary solution.
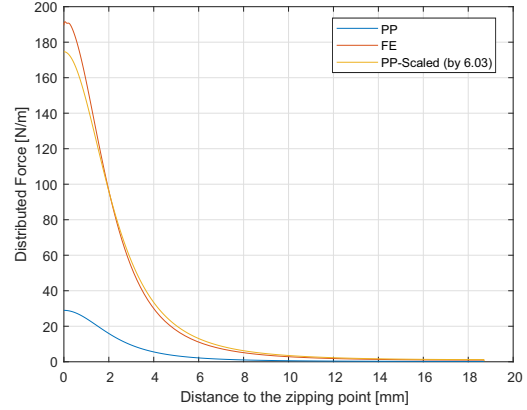

Fig. 7. Distributed force of proposed electrostatic force model (PP) against results obtained from a Finite Element (FE) computation at 2 mm displacement and 5 kV potential between electrodes.

The simulated force was expected to be higher than the experimental data as the model was idealized for an actuator completely submerged in dielectric liquid [22]. Comparative contraction forces and force:separation relationships are shown in Figure 8.

C. Time-dependent analysis

The contraction of the actuator over time, computed by the LPM, is shown in 9. The relative zipping progress was defined as the vertical contraction of the actuator with respect to the initial stroke length, while the actuator lifted an 8 g mass with different actuation voltages against time. Figure 10 shows snapshots of the actuator profile as it zips under the application of 10 kV and a load of 8 g.

The time of actuation is in line with the experimental characterization [25]. However, qualitatively, the initial expansion of the actuator and the consistently increasing closing velocity are not in line with the experimental data [22]. These differences can originate from an idealized numerical model or from unmodeled physical phenomena such as the influence of the liquid dielectric bead on the actuator dynamics and the mass of the connections that may subtly change the shape of the beam. Other expected mismatch between experimental setting and the
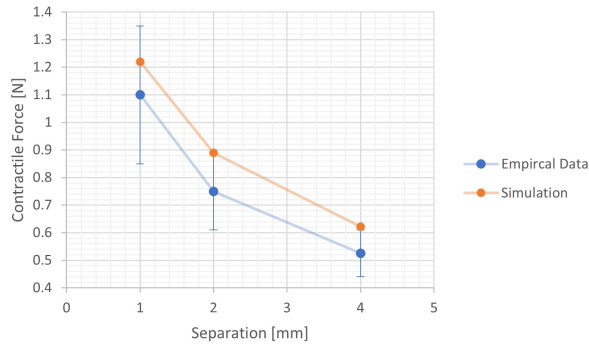
Fig. 8. Simulated contractile force, using the scaled PP model, at electrode seperations of 1 mm, 2 mm and 4 mm, at 6 kV.

Fig. 10. Profile of the actuator against time when zipping at 10 kV.

simulation is the increasing velocity of the end effector as it gets closer to the fully zipped configuration, which can be expected due to the displacement of the dielectric fluid not being modelled.

IV. DISCUSSION

The stationary solutions within the first two simulations analyzed by the FEA in COMSOL agree with the proposed LPM simulation model. They include the magnitude and profile of both the deformation of the flexible electrodes when loaded and the scaled electrostatic force. Figure 6 shows that the further away one gets from the calibration point of 61 g, the bigger stationary error is observed (with 4.74% error when doubling the load and 2.58% when halving it). This highlights that the shear elastic coefficient used in the model may be dependent on the local deformation of the particles.

The similarity in the distributed electrostatic force profiles, obtained from the PP model and the FEA analysis, suggests that this simple non-iterative method can predict the distributed electrostatic force of the
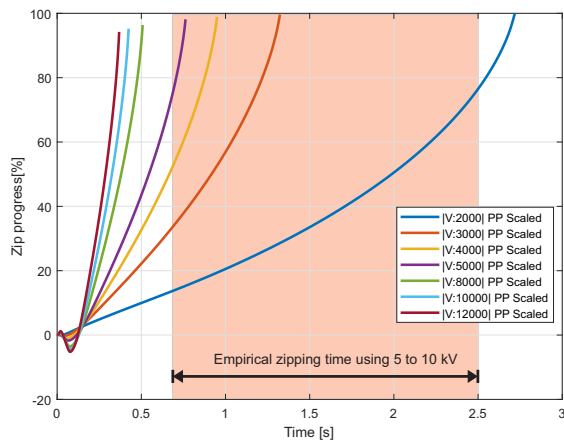

Fig. 9. Relative zipping progression over time, the red area marks approximately the empirical zipping time of an ERA with 5 to 10 kV.
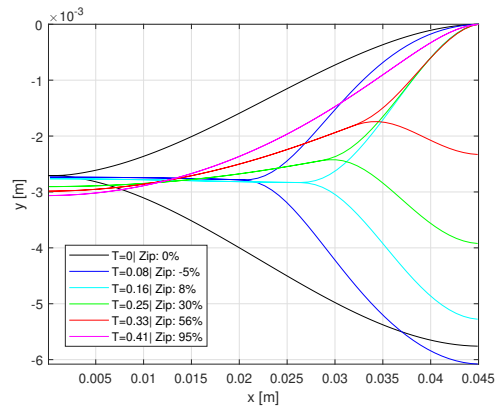
ERA, but an amplification factor (6.03 in this study) should be applied. Further research should be conducted to validate the ranges of applicability of the amplification factor, and to study the effect of the mobile dielectric liquid bead to obtain a reliable model without using FEA for calibration.

Comparing the contractile force of ERA obtained from the simulation with the experimental data [22] (Figure 8), although the simulation result falls statistically within the experimental data ranges, it is consistently higher than the mean data. The explanation for this is that the simulation idealized the ERA as being fully immersed in dielectric liquid. It has been experimentally shown that a liquid bead provided 92% of the electrostatic force compared with a fully submerged actuator [22].

A complete model needs to include the simulation of dielectric liquid dynamics, dielectrophoresis and their effect on the progressive zipping of the actuator. This may be one of the factors that caused deviation between zipping progression over time in the simulation compared to experiments, or inaccuracies in the inertial effect that are known to be hard to capture by mass-spring models [8]. Additionally the implementation of the electrostatic force model can be applied to develop ERA simulations by combining it with recent faster than real-time mass-spring models.

The mathematical framework in the proposed mechanical model allows the simulation of similar beam-like structures with large deflections, and can be translated into other soft robotic technologies such as IPMCs [26], however, only bending in one direction and stretching were included in the model excluding torsion and bending in other directions. A deeper analysis on the limitations of the proposed model would be useful to define the boundaries within which this method can be applied as differences in the zipping progress dynamics have been observed with respect to empirical studies. Analysing the response of alternative models such as more sophisticated mass-spring models using the proposed electrostatic model is a logical next step

in research. The code for the proposed mechanical and electrostatic model implemented in MATLAB can be found in the GitHub at https://github.com/ul18363/ElectroRibbon_LumpedParameter_Simulation.

Some suggested lines of research on improvements to the current model include consideration of physical phenomena such as vibrations and force propagation within the material. These may be introduced by the addition of local damping. However, this should be validated through vibration analysis, which was out of the scope for this study. Furthermore, plastic deformations can be introduced to simulate permanent bending or elongations across the beam by changing the natural length between particles in the model and offsetting the orientation of the local directions of the beam, shown in Figure 4.

V. CONCLUSIONS

This work proposed a model to simulate a soft high-performance electro-ribbon actuator by combining a lumped-parameter mass-spring model with a simplified distributed electrostatic force model. We demonstrate accurate results in stationary settings for the mechanical modelling, the contractile force and electrostatic distributed force. For dynamic modelling, qualitative deviations on the behaviour of the actuator are observed. The proposed model achieved relative deformation errors below 5% with respect to FEA results obtained from COMSOL and contractile forces in line with the experimental observations. This work presents an intuitive model for electro-ribbon and other beam-like electrically zipped actuators, which is useful to further develop and simulate more complex structures for advanced soft actuators in the future.

References

[1] S. Rich, R. Wood and C. Majidi, "Untethered soft robotics", Nature Electronics, vol. 1, no. 2, pp. 102-112, 2018.

[2] N. El-Atab et al., "Soft Actuators for Soft Robotic Applications: A Review", Advanced Intelligent Systems, p. 2000128, 2020.

[3] A. Ghosh et al., "Stimuli-Responsive Soft Untethered Grippers for Drug Delivery and Robotic Surgery", Frontiers in Mechanical Engineering, vol. 3, 2017.

[4] Duckett, T., Pearson, S., Blackmore, S., Grieve, B., & Smith, M. (2018). White paper - Agricultural Robotics: The Future of Robotic Agriculture

[5] S. Kriegman et al., "Scalable sim-to-real transfer of soft robot designs", 2020 3rd IEEE International Conference on Soft Robotics (RoboSoft), 2020.

[6] Austin, R. Corrales-Fatou, S. Wyetzner and H. Lipson, "Titan: A Parallel Asynchronous Library for Multi-Agent and Soft-Body Robotics using NVIDIA CUDA", 2020 IEEE International Conference on Robotics and Automation (ICRA), 2020.

[7] L. Marechal, P. Balland, L. Lindenroth, F. Petrou, C. Kontovounisios and F. Bello, "Toward a Common Framework and Database of Materials for Soft Robotics", Soft Robotics, 2020.

[8] W. Huang, X. Huang, C. Majidi and M. Jawed, "Dynamic simulation of articulated soft robots", Nature Communications, vol. 11, no. 1, 2020.

[9] Hiller and H. Lipson, "Dynamic Simulation of Soft Multimaterial 3D-Printed Objects", Soft Robotics, vol. 1, no. 1, pp. 88-101, 2014. Available: 10.1089/soro.2013.0010 [Accessed 31 January 2021].

[10] G. Gu, U. Gupta, J. Zhu, L. Zhu and X. Zhu, "Modeling of Viscoelastic Electromechanical Behavior in a Soft Dielectric Elastomer Actuator," in IEEE Transactions on Robotics, vol. 33, no. 5, pp. 1263-1271, Oct. 2017.

[11] Z. Wang, Bin He, Q. Wang and Y. Yin, "Electromechanical bending behavior study of soft photocurable ionogel actuator using a new finite element method", Smart Materials and Structures, vol. 25, no. 9, p. 095018, 2016.

[12] A. Mendizabal, P. Márquez-Neila and S. Cotin, "Simulation of hyperelastic materials in real-time using deep learning", Medical Image Analysis, vol. 59, p. 101569, 2020.

[13] M. Bergou, M. Wardetzky, S. Robinson, B. Audoly and E. Grinspun, "Discrete elastic rods", ACM SIGGRAPH 2008 papers on - SIGGRAPH '08, 2008. Available: 10.1145/1399504.1360662 [Accessed 26 January 2021].

[14] M. Bergou, B. Audoly, E. Vouga, M. Wardetzky and E. Grinspun, "Discrete viscous threads", ACM Transactions on Graphics, vol. 29, no. 4, pp. 1-10, 2010. Available: 10.1145/1778765.1778853 [Accessed 26 January 2021].

[15] S. Nejad, D. Gladwin and D. Stone, "A systematic review of lumped-parameter equivalent circuit models for real-time estimation of lithium-ion battery states", Journal of Power Sources, vol. 316, pp. 183-196, 2016.

[16] F. LIANG and H. LIU, "A Closed-Loop Lumped Parameter Computational Model for Human Cardiovascular System", JSME International Journal Series C, vol. 48, no. 4, pp. 484-493, 2005.

[17] Z. Duanmu, M. Yin, X. Fan, X. Yang and X. Luo, "A patient-specific lumped-parameter model of coronary circulation", Scientific Reports, vol. 8, no. 1, 2018.

[18] W. Zhang, "Dynamic modeling of coupled systems in the high-speed train", Dynamics of Coupled Systems in High-Speed Railways, pp. 55-181, 2020. Available: 10.1016/b978-0-12-813375-0.00002-9 [Accessed 27 January 2021].

[19] I. Giorgio and D. Del Vescovo, "Non-Linear Lumped-Parameter Modeling of Planar Multi-Link Manipulators with Highly Flexible Arms", Robotics, vol. 7, no. 4, p. 60, 2018.

[20] İ. Devecıoğlu and B. Güçlü, "Asymmetric response properties of rapidly adapting mechanoreceptive fibers in the rat glabrous skin", Somatosensory & Motor Research, vol. 30, no. 1, pp. 16-29, 2012.

[21] Marzbanrad and M. Pahlavani, "A System Identification Algorithm for Vehicle Lumped Parameter Model in Crash Analysis", International Journal of Modeling and Optimization, pp. 163-166, 2011.

[22] M. Taghavi, T. Helps and J. Rossiter, "Electro-ribbon actuators and electro-origami robots", Science Robotics, vol. 3, no. 25, p. eaau9795, 2018.

[23] S. Bluett, T. Helps, M. Taghavi and J. Rossite, "Self-Sensing Electro-Ribbon Actuators", IEEE Robotics and Automation Letters, vol. 5, no. 3, pp. 3931-3936

[24] Richard Suphapol Diteesawat, Aaron Fishman, Tim Helps, Majid Taghavi, Jonathan Rossiter, "Closed-loop Control of Electro-ribbon Acutators", Frontiers in Robotics and AI, Vol. 7, p. 144,2020.

[25] Taghavi, Majid, Tim Helps, and Jonathan Rossiter. "Characterisation of Self-locking High-contraction Electro-ribbon Actuators." 2020 IEEE International Conference on Robotics and Automation (ICRA). IEEE, 2020.

[26] M. Hao, Y. Wang, Z. Zhu, Q. He, D. Zhu and M. Luo, "A Compact Review of IPMC as Soft Actuator and Sensor: Current Trends, Challenges, and Potential Solutions From Our Recent Work", Frontiers in Robotics and AI, vol. 6, 2019.